16

pH Dependent Hydrothermal Synthesis and Photoluminescence of Gd_2O_3:Eu Nanostructures

Kyung-Hee Lee, Yun-Jeong Bae and Song-Ho Byeon*
Department of Applied Chemistry, Kyung Hee University
Republic of Korea

1. Introduction

The size and shape of nanocrystals (nanospheres, nanorods, nanotubes, and nanowires) are crucial parameters for controlling nanocrystal properties such as electrical transport, optical, and magnetic properties. (Hu al., 1999; Kazes et al., 2002) In particular, one-dimensional structures are the fundamental units for anisotropic shape control, presenting general shape and assembly control strategies for more complex structures. The most exciting and rapidly expanding field would be carbon nanotubes from graphite by the rolling of graphen sheets.(Ebbesen & Ajayan, 1992; Iijima, 1991; Iijima & Ichihashi, 1993; Rao et al., 2004) The MX_2 layers of metal dichalcogenides (M = Mo, W and X = S, Se) are analogous to the single graphene sheets, being able to roll into curved structures. Considerable progress has been made in the synthesis of the fullerene and nanotube structures of MX_2.(Parilla et al., 1999; Rao & Nath, 2003; Tenne, 1995) Nanorods (or nanoneedles) and nanowires have also been extensively explored because the functional nanomaterials with a restricted dimension offer the opportunities for investigating the influence of shape and dimensionality on the physical properties.(El-sayed, 2001; Xia et al., 2003) For instance, ZnO nanowire sensitized by narrow band-gap materials have been studied for use in photovoltaic device applications due to their facile synthesis and excellent optical properties.(Birkmire & Eser, 1997; Law et al., 2005; Levy-Clement et al., 2005; Leschkies et al., 2007) The selective synthesis of such structures can be achieved by a morphology control in the crystallization process including nucleation and growth. Various synthetic methods have been developed for many important materials.
The interest in studying lanthanide oxides and hydroxides stems from their potential applications including dielectric materials for multilayered capacitors, luminescent lamps and displays, solid-laser devices, optoelectronic data storages, waveguides, and heterogeneous catalysts.(Cutif et al., 2004) Recently, lanthanide-doped oxide nanoparticles are of special interests as potential materials for an important new class of nanophosphors. For instance, when the oxide nanophosphors are applied for a fluorescent labeling, there are several advantages such as sharp emission spectra, long life times, and high resistance against photobleaching in comparison with conventional organic fluorophores and quantum dots.(Beaurepaire et al., 2004; Louis et al., 2005) Many lanthanide-doped oxides generate visible light in fluorescent lamps and emissive displays. Excitation of photoluminescent phosphors takes place using ultraviolet (UV) photons generated by a

Source: Nanowires Science and Technology, Book edited by: Nicoleta Lupu,
ISBN 978-953-7619-89-3, pp. 402, February 2010, INTECH, Croatia, downloaded from SCIYO.COM

discharge in fluorescent lamp or plasma display panel (PDP). Cathodoluminescence, thermoluminescence, and electroluminescence of phosphors are also important for cathode-ray tube (CRT), field emission display (FED), radiation detector, and electroluminescence display (ELD) applications.(Yen et al., 2007) An improved performance of displays and lamps requires high quality of phosphors for sufficient brightness and long-term stability. In practice, a densely packed layer of small size particles can improve aging problems. On the other hand, when the particle is smaller than a critical value, the luminescence efficiency decreases because of increased light reabsorption and the luminescence quenching by the surface layer. Thus, high-concentration of surface defects and microstrains could greatly reduce the total luminescent intensity of nanosized luminescent materials. The concentration quenching ranges of activators are also different from those of corresponding bulk materials.(Duan et al., 2000; Zhang et al., 2003) Therefore, the morphology and size, the stoichiometry and composition, and the surface characteristics must be controlled in order to achieve the desirable objectives of improved nanophosphors.

As one of lanthanide oxides and hydroxides, Gd_2O_3 nanopaticle is a promising host matrix for multiphoton and up-conversion excitation.(Guo et al., 2004; Hirai & Orikoshi, 2004; Zhou et al., 2003) The gadolinium oxide doped with Eu^{3+} (Gd_2O_3:Eu) exhibits paramagnetic behavior (S = 7/2) as well as strong UV and cathode-ray excited luminescences, which are useful in biological fluorescent label, contrast agent, and display applications.(Blasse & Grabmaier, 1994; Goldys et al., 2006; Nichkova et al., 2005) Very recently, the magnetic resonance relaxation property of the colloidal solution of layered gadolinium hydroxide exhibited the sufficient positive contrast effect for magnetic resonance imaging (MRI).(Lee et al., 2009) In addition, Gd_2O_3:Eu is a very efficient X-ray and thermoluminescent phosphor.(Rossner & Grabmaier, 1991; Rossner, 1993) Diverse preparation methods have been developed to reduce the reaction temperature and achieve a small particle size of high quality Gd_2O_3:Eu phosphors.(Erdei et al., 1995; Ravichandran et al., 1997; Shea et al., 1996; Yan et al., 1987)

In an attempt to produce various inorganic materials in the form of isotropic or anisotropic nanostructures, the solvothermal reaction has widely been adopted due to its simplicity, high efficiency, and low cost. The hydrothermal synthetic routes to the nanostructures of lanthanide hydroxides are well introduced in the literatures. The hydrothermal treatments for colloidal precipitates of lanthanide hydroxides resulted in diverse nanostructures such as nanospheres, nanorods, nanowires, nanoplates, nanotubes, and nanobelts.(Wang et al., 2003; Wang & Li, 2002; Wang & Li, 2003) It is noted that the hydrothermal reaction is generally sensitive to the temperature, pH, or aging conditions. Thus, when we apply the hydrothermal technique to synthesize $Gd(OH)_3$:Eu as a precursor for Gd_2O_3:Eu nanophosphor, a strong pH dependence is observed in particle shape. In this chapter, we introduce a selectively controlled low-temperature hydrothermal synthesis of $Gd(OH)_3$:Eu phosphor at different pHs and subsequent dehydration into Gd_2O_3:Eu in the form of nanorods with different aspect ratios, nanowires, nanospheres, and nanotubes.(Bae et al., 2009; Lee et al., 2009) Because the concentration quenching behavior has not yet been well investigated for the phosphor nanowires, a better understanding is required for the parameters affecting the radiative or nonradiative relaxation behaviors in nanowire structures. Therefore, the growth behavior and photoluminescence property of high quality nanowires of Gd_2O_3:Eu phosphor are also described here. $Gd_{2-x}Eu_xO_3$ solid solution is examined to get an insight for the relationship between the quenching concentration of activator (Eu^{3+}) and the optimum photoluminescence characteristics of nanowires with high aspect ratio.

2. Hydrothermal synthesis of Gd_2O_3:Eu phosphor

2.1 pH dependent hydrothermal synthesis

Several shapes (i.e. nanospheres, nanorods, nanotubes, and nanowires) of $Gd(OH)_3$:Eu nanoparticles are synthesized at different pHs by using the hydrothermal method. Thus, the shape selective synthesis of $Gd(OH)_3$:Eu from nanorods with considerably different aspect ratios to nanowires, nanospheres, and nanotubes can be successively achieved with increasing the pH of initial solution for hydrothermal reaction from about 6 to 14. In a typical synthesis, the stoichiometric amounts of Gd_2O_3 and Eu_2O_3 are dissolved in HNO_3 solution. After clear solution is formed by uniform stirring, aqueous KOH solution is added until the pH of solution is adjusted to be in the range of 6 ~ 14 for the formation of colloidal hydroxide precipitates. For the hydrothermal growth of $Gd(OH)_3$:Eu particles, the resulting colloidal mixture is put into a Teflon-lined stainless steel autoclave at room temperature. The autoclave is then sealed and maintained at 120 – 180°C for several hours. In general, the solution is continuously stirred during the hydrothermal treatment. But the reaction can be performed without stirring for aging. After the reaction is completed, the solid product $Gd(OH)_3$:Eu is collected by filtration, washed with distilled water, and dried. Subsequent dehydration of $Gd(OH)_3$:Eu by heating at 500°C for several hours yields Gd_2O_3:Eu oxide. To maintain the morphology of $Gd(OH)_3$:Eu, the heating rate is controlled at slower than 3 °C /min. In order to compare the crystallization, morphology change, and luminescence behaviors at different temperatures, the additional heat treatments for all Gd_2O_3:Eu powders are successively carried out at 700 and 800 °C for several hours.

It is noted that the precipitates showing a plate-type morphology are obtained after hydrothermal treatment at pH < 7, such products show an X-ray powder diffraction (XRD) pattern quite different from that of $Gd(OH)_3$. Recently, it was reported that $Gd_2(OH)_5(NO_3)$ nH_2O of layered rare-earth hydroxide structure is obtained in the range of pH = 6 ~ 7.(Lee & Byeon, 2009) Because large capacity and high affinity for the ion-exchange reaction, this compound can be used as host materials for a wide range of active molecules. Fig. 1 shows typical XRD patterns of the as-synthesized $Gd_2(OH)_5(NO_3)$ nH_2O:Eu at pH ~ 7, $Gd(OH)_3$:Eu from hydrothermal process at pH ~ 8 (nanorods; see section 3.1) and ~ 11 (nanowires; see section 3.1), and Gd_2O_3:Eu obtained after heat treatment at 500 °C. A series of strong (00*l*) reflections observed in the XRD pattern of $Gd_2(OH)_5(NO_3)$ nH_2O:Eu (Fig. 1a) is characteristic of a layered phase and corresponding to an interlayer separation of ~ 8.5 Å. In contrast, all the reflections for $Gd(OH)_3$:Eu and Gd_2O_3:Eu can be indexed to the hexagonal (space group $P6_3/m$; Figs. 1b and 1c) and the cubic (space group $Ia3$; Fig.1d) phases respectively.(JCPDS card 83-2037; Buijs et al., 1987) While $Gd(OH)_3$:Eu obtained at pH ~ 8 is well crystallized, the increase of solution pH to ~ 11 and ~ 13 results in a relatively weak and broad intensity patterns, indicating a poorer crystallinity. The full-widths at half-maximum (FWHM) of the (110), (101), (201) reflections of $Gd(OH)_3$:Eu obtained at pH ~ 8 are smaller than one half in comparison with those obtained at pH ~ 11. Furthermore, it is of particular interest that the relative intensities of (110) and (101) diffractions for $Gd(OH)_3$:Eu are significantly different depending on the solution pH for hydrothermal synthesis. The intensity ratios between (110) and (101) reflections of the hydroxide nanorod is around 0.5 (Fig. 1b). Similar XRD patterns are observed for $Gd(OH)_3$:Eu oxides which are prepared at different pHs other than ~ 11 and the (110)/(101) intensity ratios are typically in the range of 0.5 ~ 1.0. These observations are consistent with the previously reported results for

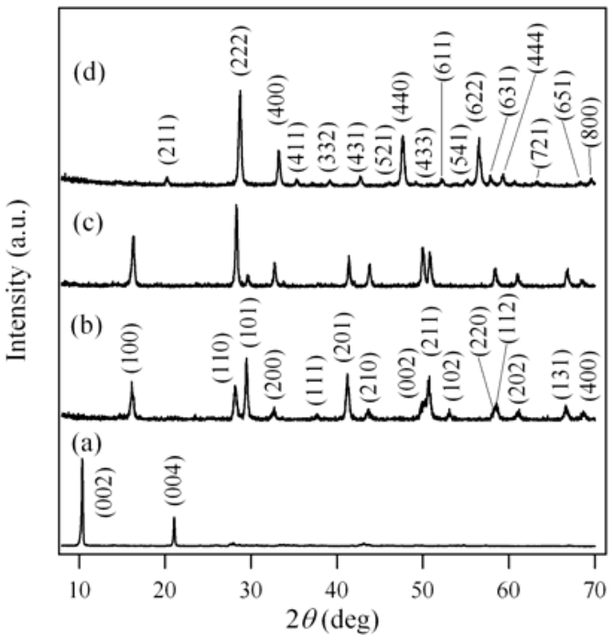

Fig. 1. Powder X-ray diffraction patterns of $Gd(OH)_5(NO_3)$ nH_2O:Eu and $Gd(OH)_3$:Eu prepared by hydrothermal reaction at 180 °C and pH ~ (a) 7, (b) 13 (nanorods), and (c) 11 (nanowires) and (d) Gd_2O_3:Eu obtained after dehydration at 500 °C.

$Gd(OH)_3$.(Wang & Li, 2002; Wang et al., 2003; Louis et al., 2003) In contrast, such intensity ratio dramatically increased up to ~ 8 in the XRD pattern of the hydroxide prepared at pH ~ 11 (Fig. 1c). This would suggest that the (110) orientation is strongly preferred for $Gd(OH)_3$:Eu prepared at around this pH range. The comparison of the XRD patterns and morphology changes of $Gd(OH)_3$:Eu (see section 3.1) indicates that the growth direction of $Gd(OH)_3$:Eu from nanorods to nanowires is parallel to the (110) planes. Some more details are discribed in the next section.

2.2 Synthesis of high quality nanowires of Gd_2O_3:Eu at constant pH

The careful adjustment of pH for the hydrothermal reaction is required to induce well developed nanowire structure with sufficiently high aspect ratio. In contrast to the synthesis of lanthanide phosphate nanowires at pH = 1 – 2 under the hydrothermal condition,(Fang et al., 2003) the optimal pH range for the growth of $Gd(OH)_3$:Eu nanowires is close to around 11. Nanowires of $Gd_{1-x/2}Eu_{x/2}(OH)_3$ solid solution (x = 0.08, 0.12, 0.16, 0.20, and 0.24) are accordingly synthesized at pH ~ 11 by the procedure similar to section 2.1. The high quality bulk powder of Gd_2O_3:Eu phosphor can be prepared according to the citrate route.(for example, see Byeon et al., 2002)

It is well known that, besides pH, the concentration of solution can also strongly affect the transport behavior of constituting ions and the growth behavior of particles in the solvothermal synthesis. Thus, the highly anisotropic growth to the more uniform nanowires with several tens of micrometers in length is achieved by maintaining the higher concentration of the precursors dissolved in the initial HNO_3 solution for hydrothermal synthesis. The temperature is another factor influencing the growth of $Gd(OH)_3$:Eu

nanowires. For instance, no nanowire is induced below 120 °C. The nanorods with relatively high aspect ratios are obtained at 120 – 160 °C under the same pH condition. The growth of nanowires longer than 10 micrometers can be achieved by raising the reaction temperature above 160 °C. Fig. 2 compares the XRD pattern of $Gd(OH)_3$:Eu bulk powder with those of the as-synthesized hexagonal $Gd(OH)_3$:Eu nanowires from hydrothermal process at pH ~ 11 and the cubic Gd_2O_3:Eu nanowires obtained after heat treatment at 500 °C. Similarly to the case in section 2.1, the intensity ratio between (110) and (101) reflections for the hydrothermally synthesized $Gd(OH)_3$:Eu nanowires are significantly different from those of the bulk powder; such relative intensity ratio of the bulk hydroxide is close to 1.0 (Fig. 2a), which is significantly smaller than that (~8) of the hydroxide nanowire (Fig. 2b). Single crystalline nanowires of hydroxides and oxides have been extensively studied.(Sharma & Sunkara, 2002; Tang et al., 2005; Singh et al., 2007) Their formations are related to the fact that the growth rate along one crystallographic direction is significantly faster than along the other directions. It has been reported that the growth direction of $Gd(OH)_3$ to nanorods is parallel to the (110) planes of the hexagonal unit cell.(Du & van Tendeloo, 2005) High resolution transmission electron microscope (HRTEM) images of $Gd(OH)_3$:Eu nanorod and nanowire are compared in Fig. 3. The fine fringes demonstrate that the as-synthesized $Gd(OH)_3$:Eu nanorods and nanowires are single crystalline. The spacing between fringes along both the rod and wire axes is about 0.32 nm which is close to the interplanar spacing of the (110) plane. This agreement confirms that the exceptionally high (110)/(101) intensity ratio of nanowires (Fig. 2b) is attributed to the preferential growth of nanowire parallel to the (110) planes. Although $Gd(OH)_3$ nanorods with relatively high aspect ratios have been described as nanowires in the literatures, true nanowires would show highly increased (110)/(101) intensity ratios in their XRD patterns.

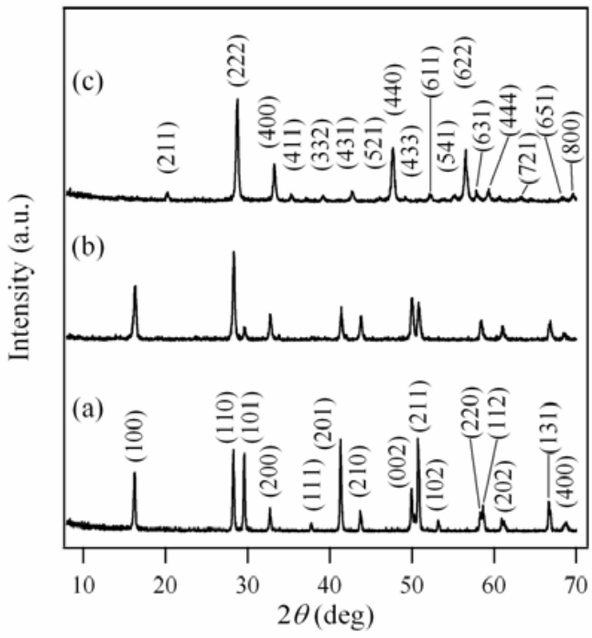

Fig. 2. Powder X-ray diffraction patterns of (a) the bulk $Gd(OH)_3$:Eu powder, (b) as-synthesized $Gd(OH)_3$:Eu nanowires from hydrothermal reaction, and (c) Gd_2O_3:Eu nanowires obtained after dehydration at 500 °C.

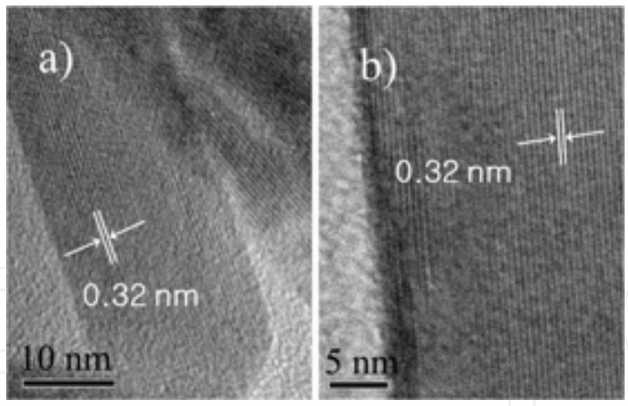

Fig. 3. HRTEM photographs of $Gd(OH)_3$:Eu prepared by hydrothermal reaction at 180 °C. pH ~ (a) 13 (nanorods) and (b) 11 (nanowires).

3. Morphological aspects of Gd_2O_3:Eu nanophosphor

3.1 pH dependent shape evolution of $Gd(OH)_3$:Eu and Gd_2O_3:Eu

The selective synthesis of diverse nanomaterials is challenging for understanding physical properties derived from well difined shape dimensionality. For example, the anisotropic growth of lanthanide orthophosphates ($LnPO_4$ where Ln = lanthanides) nanostructure can be enhanced by kinetically controlled hydrothermal processes using carefully selected chelating ligands.(Yan et al., 2005) Among many parameters affecting the solvothermal synthesis, the adjustment of pH was found to play a key role in selectively controlling the morphology of $Gd(OH)_3$:Eu nanostructures. In particular, KOH would influence on the nucleation and anisotropic growth of particles. For instance, the layered gadolinium hydroxynitrate $Gd_2(OH)_5(NO_3)\cdot nH_2O$:Eu is obtained at pH = 6 – 7. The field emission scanning electron microscopy (FE-SEM) image (Fig. 4a) of $Gd_2(OH)_5(NO_3)\cdot nH_2O$:Eu obtained at pH ~ 7 shows that they comprise a plate-like microcrystalline powders. Because of very weak intensity and insufficient number of non-(00*l*) reflections observed in XRD patterns of $Gd_2(OH)_5(NO_3)\cdot nH_2O$:Eu (Fig. 1a), the arrangement mode within the *ab* plane is measured by the selected area electron diffraction (SAED). As shown in Fig. 4b, the clear spots observed in the reciprocal lattice, which are rectangularly arranged, confirm an order within the *ab* plane of crystals (a ~ 7.3 Å, b ~ 12.9 Å).

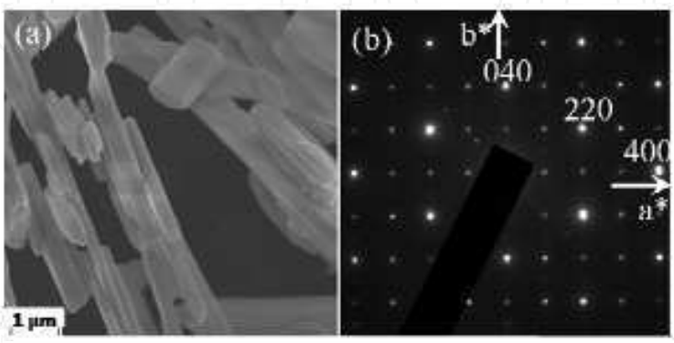

Fig. 4. (a) FE-SEM photograph and (b) selected area elctron diffraction patterns of $Gd_2(OH)_5(NO_3)\cdot nH_2O$:Eu prepared by hydrothermal reaction at 180 °C, pH ~ 7.

On the contrary, at pH > 8, $Gd(OH)_3$:Eu particles are produced in the form of nanorods with variable aspect ratios, nanowires, or the mixture of nanosheets, nanotubes, and nanorods, depending on the solution pH. Fig. 5 shows FE-SEM images of $Gd(OH)_3$:Eu synthesized at pH ~ 8 and Gd_2O_3:Eu obtained by subsequent heat treatment at 500 and 800 °C. It can be seen in Fig. 5a that the as-synthesized $Gd(OH)_3$:Eu are composed of highly uniform nanorods. The aspect ratio of nanorods is tunable by controlling the experimental conditions of pH, temperature, and concentration. After dehydrating this hydroxide to Gd_2O_3:Eu at high temperatures up to 800 °C, the nanorod shape is completely retained as shown in Figs. 5b and 5c. It has already been reported that the nanorod shape of $Gd(OH)_3$:Eu is maintained after the dehydration into Gd_2O_3:Eu.(Chang et al., 2005) Their average diameter and length are around 200 nm and 1 – 1.5 μm, respectively. The morphology of $Gd(OH)_3$:Eu synthesized at pH ~ 9 is shown in Fig. 6a. This powder also consists of uniform rod-like particles. Compared with those obtained at pH ~ 8, the diameter of $Gd(OH)_3$:Eu nanorods is smaller but the length is longer when they are prepared at pH ~ 9.0. The nanorod structure is not collapsed after thermal dehydration (Figs. 6b and 6c). Their average diameter and length are around 150 nm and 1.5 – 2 μm, respectively.

During hydrothermal synthesis, it is revealed that the higher the pH of starting solution is, the smaller diameter of $Gd(OH)_3$:Eu nanorods is induced. In contrast, the average length of the nanorods is increased so that the aspect ratio of $Gd(OH)_3$:Eu nanorods becomes larger with the increase of solution pH at the same concentration and reaction temperature. Fig. 7 shows typical images of the as-synthesized $Gd(OH)_3$:Eu at pH ~ 10 and its dehydrated oxide

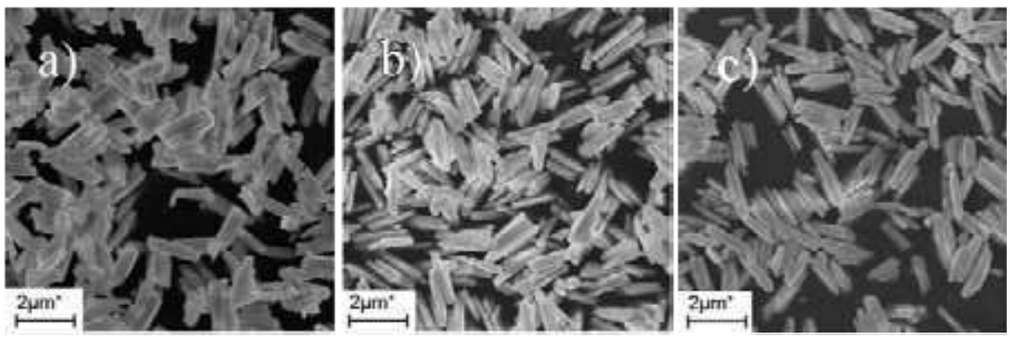

Fig. 5. FE-SEM photographs of (a) $Gd(OH)_3$:Eu prepared by hydrothermal reaction at 180 °C, pH ~ 8 and Gd_2O_3:Eu obtained after dehydration at (b) 500 °C and (d) 800 °C.

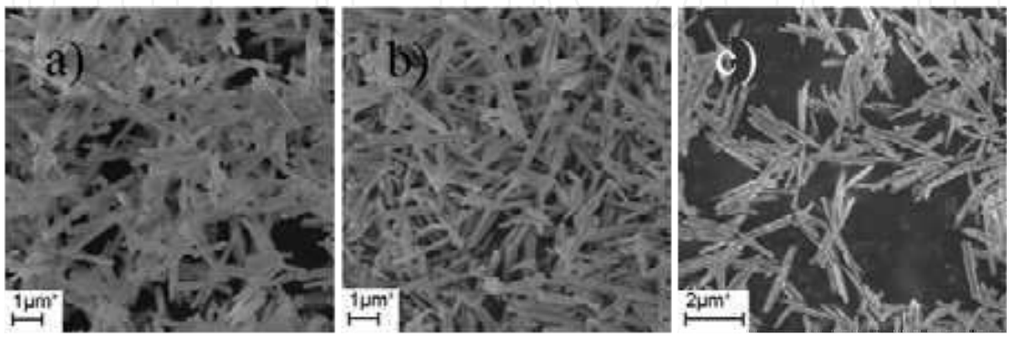

Fig. 6. FE-SEM photographs of (a) $Gd(OH)_3$:Eu prepared by hydrothermal reaction at 180 °C, pH ~ 9 and Gd_2O_3:Eu obtained after dehydration at (b) 500 °C and (d) 800 °C.

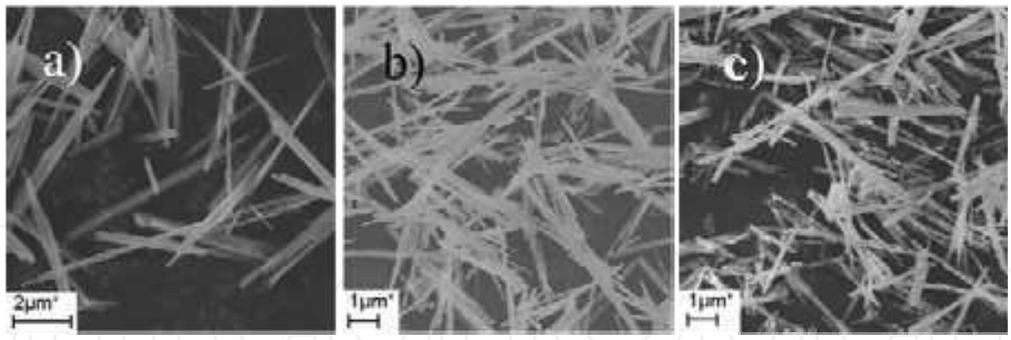

Fig. 7. FE-SEM photographs of (a) $Gd(OH)_3$:Eu prepared by hydrothermal reaction at 180 °C, pH ~ 10 and Gd_2O_3:Eu obtained after dehydration at (b) 500 °C and (d) 800 °C.

Gd_2O_3:Eu. Both compounds exhibit the nanorod structures with average diameter of about 100 nm and length of 3 – 4 μm. The maximal aspect ratios of $Gd(OH)_3$:Eu and Gd_2O_3:Eu particles are achieved in the higher pH range. The typical FE-SEM and TEM images of $Gd(OH)_3$:Eu synthesized at pH ~ 11 are shown in Figs. 8a and 8b, respectively. As can be seen in these figures, the as-synthesized $Gd(OH)_3$:Eu is composed of uniform nanowires whose lengths are close to several tens of micrometers. The images shown in Fig. 8b with higher magnification suggests that the diameters of nanowires are in the range of 20 – 30 nm. Figs. 8c and 8d display the FE-SEM of Gd_2O_3:Eu nanowires converted by thermal treatment of $Gd(OH)_3$:Eu nanowires at 500 °C and 800 °C, respectively. The temperature and activator (Eu^{3+}) concentration dependence of Gd_2O_3:Eu nanowires are additionally described in next section (3.2.). Further addition of KOH solution to adjust the pH to higher than 11 significantly reduces the aspect ratio of $Gd(OH)_3$:Eu particles to produce essentially

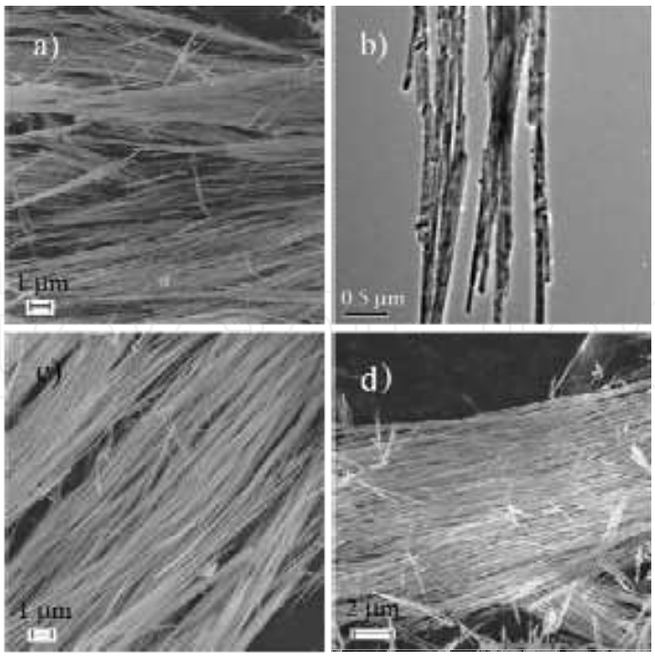

Fig. 8. FE-SEM and TEM photographs of (a and b) $Gd(OH)_3$:Eu prepared by hydrothermal reaction at 180 °C, pH ~ 11 and Gd_2O_3:Eu obtained after dehydration at (c) 500 °C and (d) 800 °C.

nanorods. The XRD pattern of this hydroxide is quite similar to Fig. 1b, the (110)/(101) intensity ratio being close to 0.7. It was proposed that the high OH^- ion concentration is preferable for the high aspect ratio but greatly reduce the ionic motion for the one-dimensional growth.(Wang & Li, 2002) This would imply that an optimal pH condition is required for the growth of true nanowires with high aspect ratio. Fig. 9a shows a FE-SEM image of the as-synthesized $Gd(OH)_3$:Eu powder by hydrothermal reaction at pH ~ 12. Although the particle shapes are uniform and wire-like, the aspect ratio is significantly decreased in comparison with that of true nanowires (Fig. 8) prepared at pH ~ 11. The morphology images of Gd_2O_3:Eu also exhibit the nanorod shapes (Figs. 9b and 9c), indicating the maintenance of morphology. The diameter and length of rigid nanorods are in the range of 20 – 30 nm and 2 – 3 μm, respectively.

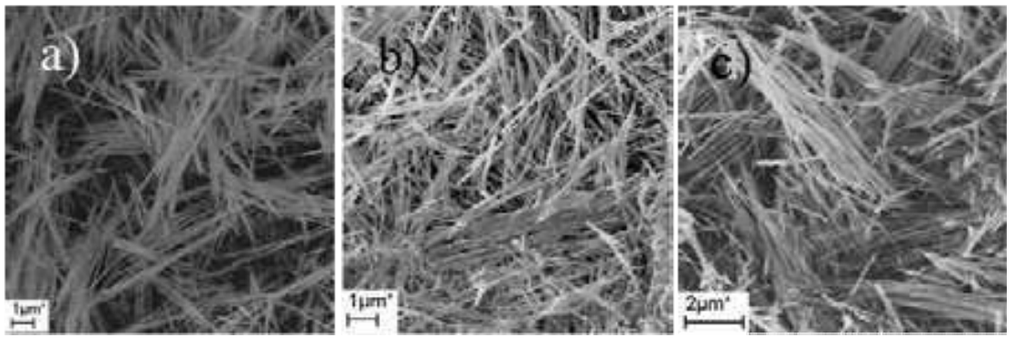

Fig. 9. FE-SEM photographs of (a) $Gd(OH)_3$:Eu prepared by hydrothermal reaction at 180 °C, pH ~ 12 and Gd_2O_3:Eu obtained after dehydration at (b) 500 °C and (d) 800 °C.

Compared with those prepared at lower pH ranges, the morphology of $Gd(OH)_3$:Eu obtained at pH ~ 13 strongly depends on the reaction temperature; the formation of nanowires is not induced but instead both nanorod and nanotube structures seems in competition in this pH range. The formation of nanorods with low aspect ratio is preferred at higher than 160 °C while the nanotubes are mainly obtained at lower than 140 °C. When the hydrothermal reaction is carried out with the initial solution of pH ~ 13, the $Gd(OH)_3$:Eu crystallites synthesized at 180 °C display the uniform morphology of nanorods with 20 – 30 nm in diameter and 200 – 300 nm in length (Fig. 10a). In contrast to the observations in other nanorods prepared at lower pHs, the morphology of $Gd(OH)_3$:Eu nanorods obtained at this pH range was not retained after the thermal transformation into Gd_2O_3:Eu. Figs. 10b and 10c are the FE-SEM and TEM images of Gd_2O_3:Eu obtained from heat treatment of $Gd(OH)_3$:Eu at 500 °C. Relatively regular Gd_2O_3:Eu particles are all quasi-spherical and the average particle size is close to 30 – 60 nm. Observation of the fine fringes supports a formation of regular crystalline lattice. On the other hand, the mixture of nanorods, nanotubes, and nanosheets is produced when $Gd(OH)_3$:Eu is synthesized at 120 °C. Fig. 10d shows that the nanotubes have outer diameters less than 30 nm and lengths of 150 – 200 nm. The nanorods have the aspect ratio smaller than that prepared at 180 °C. Considering that the nanosheets are also observed, the formation of sheet-structure is likely followed by the formation of nanotubes at a lower temperature, which in turn grows to more stable nanorods at a higher temperature. The optimal condition to synthesize uniform nanotubes of $Gd(OH)_3$:Eu is strongly dependent on the concentration of KOH and temperature. Similarly to the nanorods prepared at 180 °C, no shape is retained in the mixture of nanosheets, nanotubes,

and nanorods obtained at 120 °C but the spherical nanoparticles with size of 10 – 40 nm are mainly obtained after dehydration into Gd_2O_3:Eu (Fig. 10e). The observed fine fringes are associated with the regular crystalline lattice (Fig. 10f). The spacings between fringes, 0.32, 0.27, and 0.20 nm correspond to the interplanar spacing of the (220), (400), and (440) plane of cubic cell, respectively. The origin of collapse of this nanorod shape is not straightforward. If we consider that the nanosheet, nanorod, and nanotube morphologies are in competition, such collapse would be attributed to a metastable nanorod structure. Many different strategies for the synthesis and characterization of inorganic nanotubes have been reported.(Rao & Nath, 2003) In the majority of the cases, the nanotube structures are induced by a rolling of single sheets from the layered lattices. Some oxide nanotubes have been synthesized by employing a hydrothermal technique. For instance, the hydrothermal synthesis of single-crystalline α-Fe_2O_3 nanotubes has been accomplished.(Jia et al., 2005)

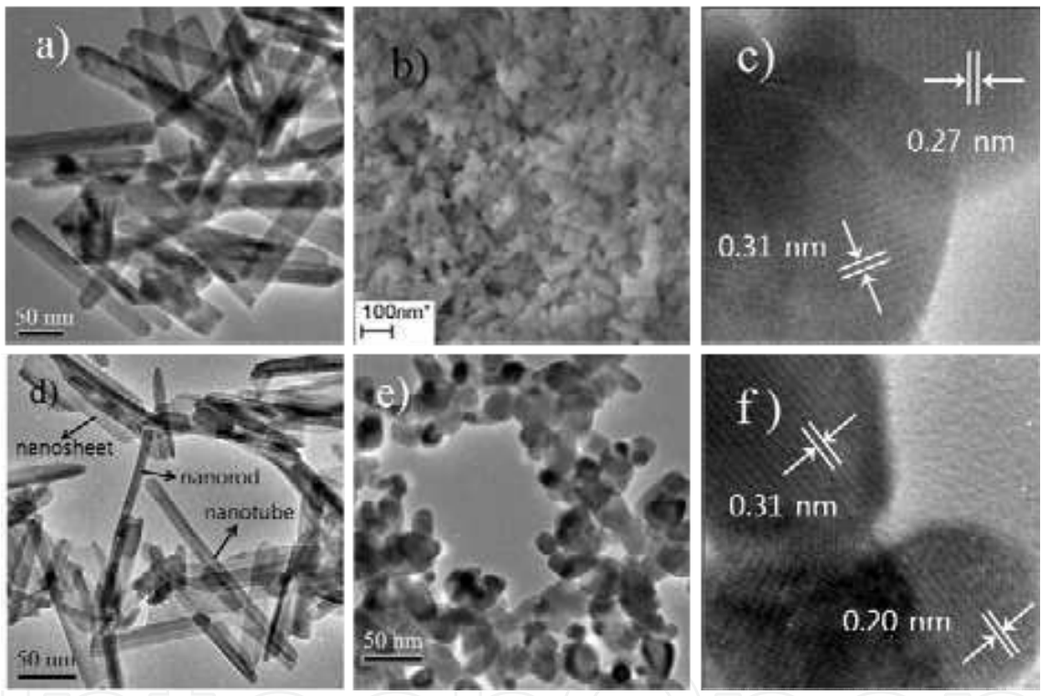

Fig. 10. FE-SEM and TEM photographs of (a) $Gd(OH)_3$:Eu prepared by hydrothermal reaction at 180 °C, pH = 12.9 and (b and c) Gd_2O_3:Eu obtained after dehydration at 500 °C. TEM photographs of (d) $Gd(OH)_3$:Eu prepared at 120 °C, pH ~ 13 and (e and f) Gd_2O_3:Eu obtained after dehydration at 500 °C.

When the direct synthesis of oxide nanotubes is difficult, a precursor prepared by hydrothermal reaction can be used under the appropriate conditions. Highly crystalline TiO_2 nanotubes were synthesized by hydrogen peroxide treatment of low crystalline TiO_2 nanotubes prepared by hydrothermal methods.(Khan et al., 2006) In particular, CeO_2 nanotubes have been prepared by the controlled annealing of the as-synthesized $Ce(OH)_3$ nanotubes from hydrothermal synthesis.(Tang et al., 2005) A similar result was expected for a thermal dehydration of $Gd(OH)_3$:Eu nanotubes to Gd_2O_3:Eu nanotubes. Unfortunately, $Gd(OH)_3$:Eu nanotubes are collapsed to yield spherical nanoparticles, no Gd_2O_3:Eu nanotubes being obtained after dehydration at 500 °C. The nanotubes of cubic Gd_2O_3:Eu,

which is not a lamella structure, will require numerous defects and twin orientation relationships, which is energetically unfavorable, during rearrangement for the structural transformation. The difference in strain and curvature between the outer and inner surfaces of nanotubes will induce a different contraction tensions around defects and twins. This torsion would consequently lead to a collapse of tube structure. The hydrothermal reaction at pH ~ 14 results in $Gd(OH)_3$:Eu nanorods with low aspect ratios. This hydroxide is not well crystallized and the rod shape is not completely retained after thermal dehydration into Gd_2O_3:Eu. Instead, the mixture of nanospheres andnanorods is obtained.

3.2 The growth behavior of Gd_2O_3:Eu nanowire

Oxide nanowires can be synthesized by diverse methods. Single crystalline cubic spinel $LiMn_2O_4$ nanowires were prepared by using $Na_{0.44}MnO_2$ nanowires as a self-template.(Hosono et al., 2009) $ZnSnO_3$ nanowires were prepared by using D-fructose as a molecule template.(Fang et al., 2009) Non-catalytic resistive heating of pure metal wires or foils at ambient conditions was developed to grow the nanowires of metal oxides.(Rackauskas et al., 2009) A vapor–solid route was employed for the catalyzed synthesis of vertically aligned V_2O_5 nanowire arrays with tunable lengths and substrate coverage.(Velazquez & Banerjee, 2009) The hydrothermal synthesis also provides an effective route to fabricate the oxide nanowires. Single-crystalline tetragonal perovskite-type PZT oxide nanowires has been synthesized by applying a polymer-assisted hydrothermal method.(Xu et al., 2005) Uniform single-crystalline $KNbO_3$ oxide nanowires have also been obtained by employing the hydrothermal route.(Magrez et al., 2006) However, a direct hydrothermal synthesis of Gd_2O_3:Eu oxide nanowires is difficult because of high stability of the hydroxide form at high pH conditions. Instead, Gd_2O_3:Eu nanowires can be obtained via dehydration of hydrothermally synthesized hydroxide forms as described in section 3.1. Fig. 11a shows again the FE-SEM image of Gd_2O_3:Eu oxide of several tens of micrometers in length. Fig. 11b with higher magnification suggests that the diameters of nanowires are in the range of 10 ~ 30 nm. It is generally expected that the highly anisotropic shapes of nanoparticles would collapse when they transform into a different structure of phase by heat treatment.(Liang & Li, 2003) In this respect, it is of interest that the nanowire shape of $Gd(OH)_3$:Eu are not broken after the transformation into Gd_2O_3:Eu structure by heat treatment. The structural transformation from hexagonal $Gd(OH)_3$ to cubic Gd_2O_3 proceeds through the formation of intermediate monoclinic GdOOH. If we consider that the single-crystalline character of $Gd(OH)_3$ nanorods is retained in GdOOH,(Chang et al., 2006) a sequential transformation from hexagonal to monoclinic and finally to cubic structure, rather than an abrupt transformation, could be responsible for the maintenance of wire-shapes in Gd_2O_3:Eu. The hydrothermal method for the synthesis of $Gd(OH)_3$:Eu nanowires consequently provides a selective route to the nanowires of red-emitting Gd_2O_3:Eu oxide nanowires. Despite the maintenance of anisotropic particle shape, however, the structural transformation of nanowires from hexagonal to cubic symmetry will require numerous defects associated with the presence of microstrains. HRTEM image of Gd_2O_3:Eu nanowires shown in Fig. 11c supports this feature. Besides the fine fringes spaced by about 0.27 nm, which is close to the interplanar spacing of the (400) plane, the other weak fringes and wave-like images likely attributed to the stacking faults are observed as indicated by dotted line in the circle of this figure. The concentration of Eu^{3+} also influences on the formation of $Gd_{1-x/2}Eu_{x/2}(OH)_3$ and consequently $Gd_{2-x}Eu_xO_3$ nanowires. SEM images of nanowires are

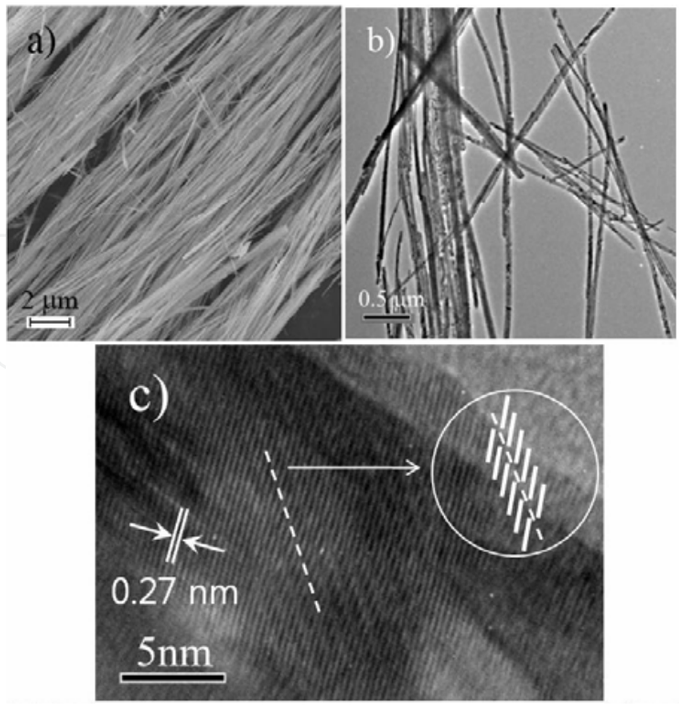

Fig. 11. (a) FE-SEM, (b) TEM, and (c) HRTEM photographs of Gd_2O_3:Eu nanowires (A stacking fault is represented in the circle.) obtained after dehydration at 500 °C.

compared as a function of Eu^{3+} concentration(x) and heating temperature in Fig. 12. As shown in these images, when the concentration of doped Eu^{3+} increases from 0.08 up to ~ 0.20, the morphology of Gd_2O_3:Eu nanowire tends to be improved. Further increase of doping concentration results in an abrupt decrease in aspect ratio and then nanorods are obtained. The nanowire morphology of Gd_2O_3:Eu is maintained even after heat treatment up to 700 and 800 °C. Partial collapse of nanowires to the irregular nanorods is induced at higher than 900 °C.

4. Photoluminescence spectra of Gd_2O_3:Eu nanophosphors

4.1 Correlation between photoluminescence and aspect ratio of Gd_2O_3:Eu nanoparticles

The optical characteristics and performances of nanometer-sized phosphor materials are generally dependent on their crystal structures, size, and morphologies. For instance, a difference of about 10 nm in the charge-transfer band position is observed between Gd_2O_3:Eu nanorods and microrods despite the same composition.(Chang et al., 2005) The correlation between morphology and photoluminescence (PL) intensity of Gd_2O_3:Eu phosphor provides an insight for a particle shape of the oxide nanophosphor with high PL efficiency. Indeed, the photoemission spectra of Gd_2O_3:Eu with different aspect ratios support that a systematic difference in PL intensity is induced as a function of the particle morphology. Fig. 13a compares the PL emission spectra of Gd_2O_3:Eu phosphors as a function of the pH value at which corresponding hydroxide precursors are synthesized. For comparison, the emission intensity measured from a commercial Y_2O_3:Eu is also plotted as a reference in the figure. The observed several emission bands are associated with the $^5D_0 - {}^7F_J$

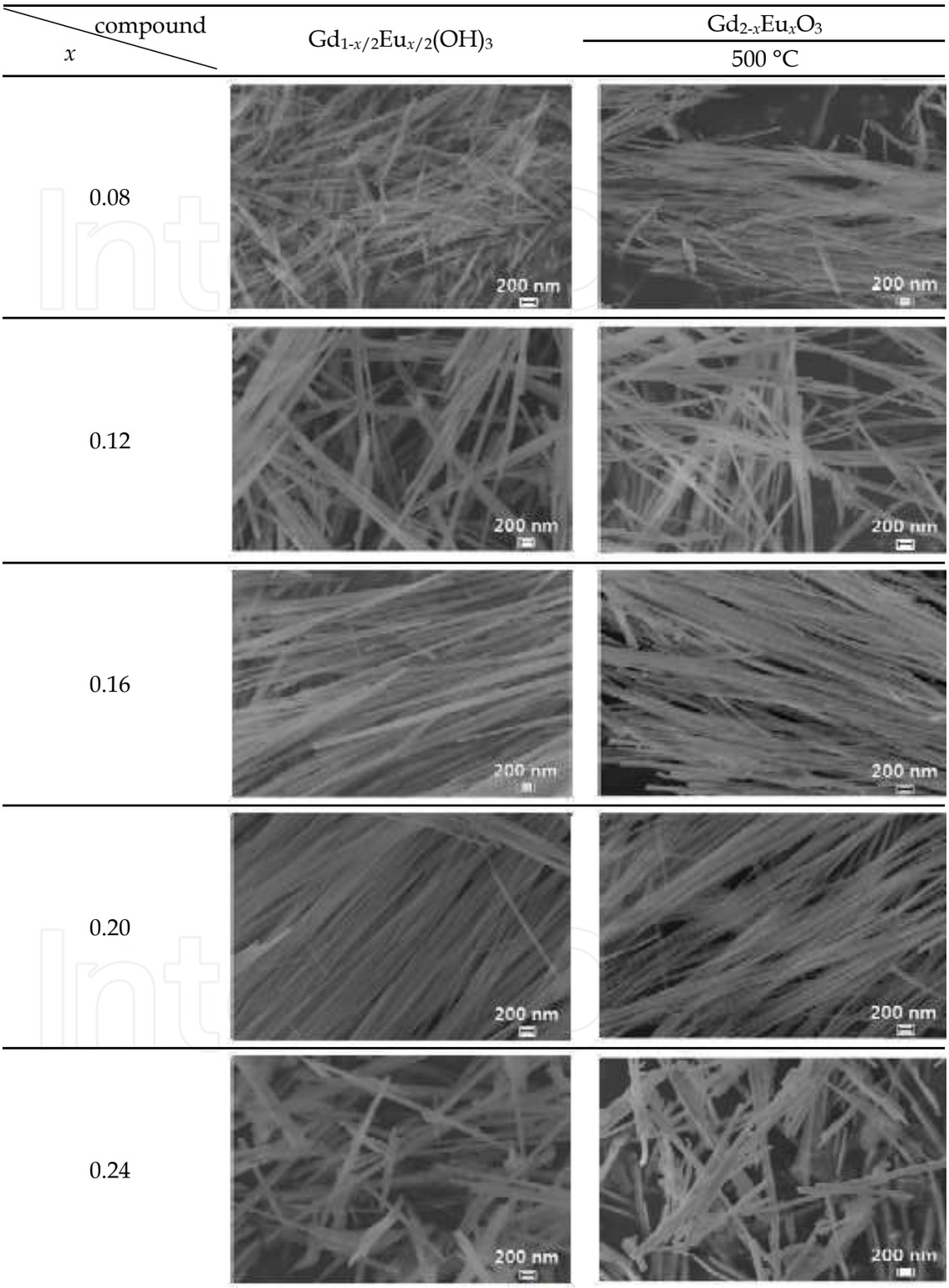

Fig. 12. Morphology evolution of $Gd_{1-x/2}Eu_{x/2}(OH)_3$ and $Gd_{2-x}Eu_xO_3$ nanowires as a function of Eu^{3+} concentration and temperature.

compound / x	$Gd_{2-x}Eu_xO_3$ 600 °C	$Gd_{2-x}Eu_xO_3$ 800 °C
0.08	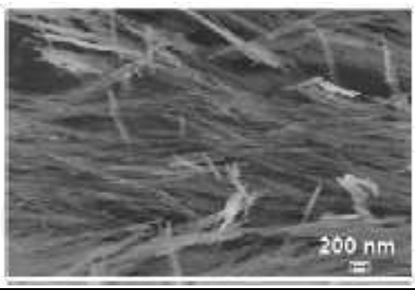	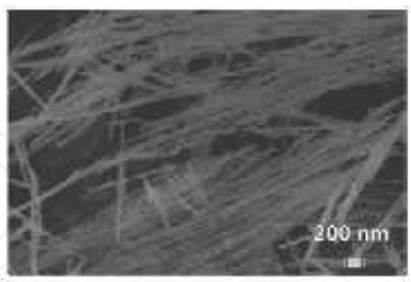
0.12	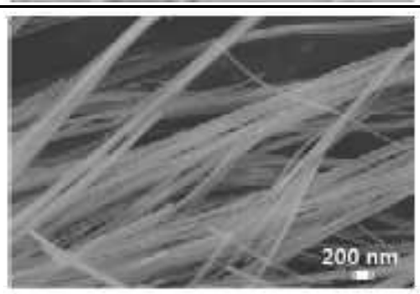	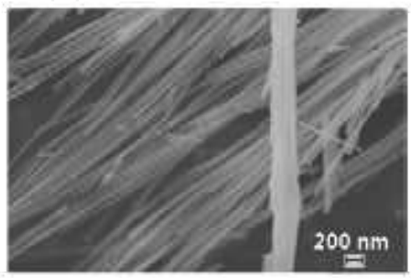
0.16	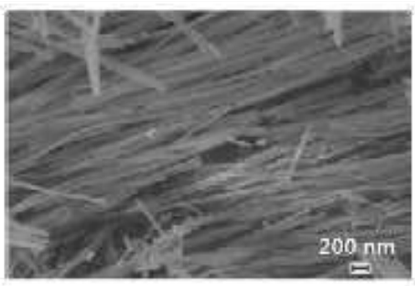	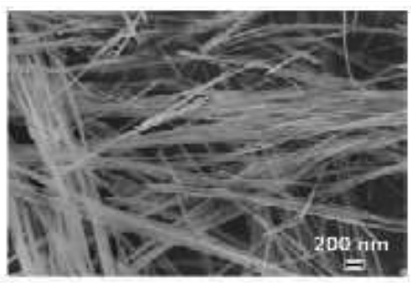
0.20	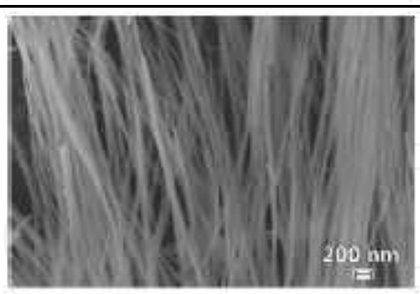	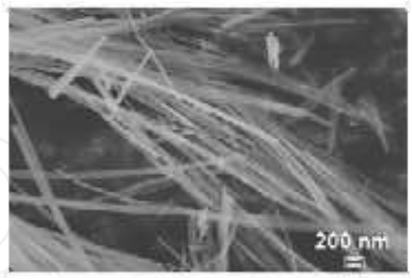
0.24	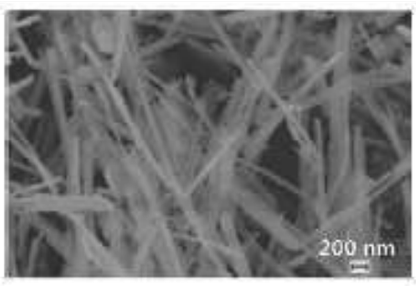	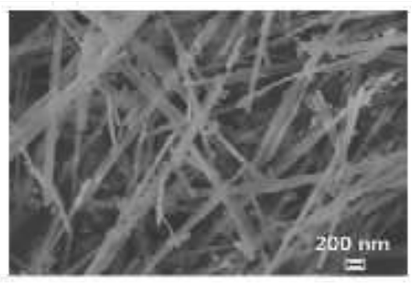

Fig. 12. (continued)

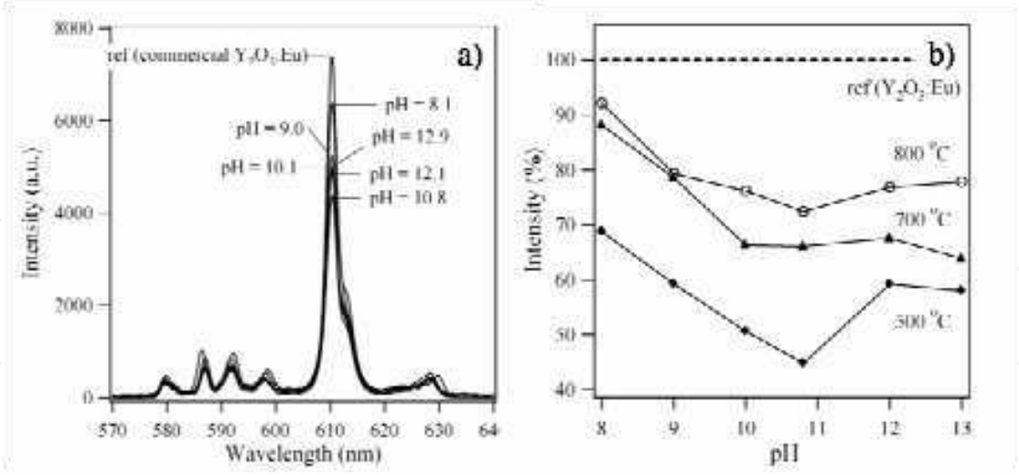

Fig. 13. (a) PL emission spectra of Gd_2O_3:Eu obtained after dehydration of $Gd(OH)_3$:Eu at 800 °C. PL emission spectrum of commercial Y_2O_3:Eu is also compared as a reference. (b) Comparison of the relative PL emission intensity of Gd_2O_3:Eu phosphors obtained after heat treatment for 5 h as a function of the solution pH for the hydrothermal synthesis. All intensities were measured as values relative to that of commercial Y_2O_3:Eu.

(J = 1 ~ 5) transitions of the Eu^{3+} ion, where the most intense emission at 610 nm is assigned to the $^5D_0$ – $^7F_2$ transition.(Brecher et al., 1967) As shown in this figure, Gd_2O_3:Eu oxide from the hydroxide prepared at pH ~ 8 exhibits strong emission whose intensity is close to 90 % in comparison with that of commercially available Y_2O_3:Eu. The commercial Y_2O_3: Eu phosphor is generally sintered at temperature above 1300 °C. An adoption of hydrolysis technique using urea for the synthesis of Y_2O_3: Eu also requires the firing temperature of 1150 – 1400 °C to achieve an optimum luminescent property.(Matijevic & Hsu, 1987; Jiang et al., 1998; Jing et al., 1999) It is accordingly notable that the emission intensity of Gd_2O_3:Eu nanorods obtained at 800 °C is comparable with that of commercial Y_2O_3: Eu. In Fig. 13b, the pH dependent PL intensities of Gd_2O_3:Eu phosphors are summarized as a function of the dehydration temperature of corresponding hydroxide precursors. The emission intensity of Gd_2O_3:Eu exhibits a minimum value when the pH for hydrothermal synthesis of the hydroxide increases. The aspect ratio of $Gd(OH)_3$:Eu (or Gd_2O_3:Eu) is enhanced with increasing the solution pH from ~ 8 to ~ 11 which is the optimal value for the formation of nanowires. In contrast, the PL emission intensity of Gd_2O_3:Eu is monotonically reduced with increase of the aspect ratio in this pH range. The lowest emission is observed with the nanowires (pH ~ 11) of the highest aspect ratio. The intensity of Gd_2O_3:Eu nanowires obtained after dehydration at 800 °C is close to 70 % in comparison with that of commercial Y_2O_3:Eu. When pH > 11, the aspect ratio of Gd_2O_3:Eu nanorods is decreased again and then the PL emission intensity is enhanced.

Comparing the PL behavior as a function of the particle morphology, the emission intensity of Gd_2O_3:Eu decreases when the aspect ratio becomes larger. One of the origins for such a correlation could be a difference in the surface area of particles. An important source of luminescence quenching in nanosized particles is the surface, where the coordination of the atoms differs from that in the bulk.(Counio et al., 1998) As a result of higher aspect ratios, the enlarged surface area of crystallites would result in an increase of surface defects which can be the nonradiative recombination centers (see section 4.2). Thus, the high concentration

of stacking faults and twins in the surface of nanowires can be an origin for a decrease of the emission intensity observed in higher aspect-ratio-particles.

4.2 Photoluminescence and quenching concentration of Gd_2O_3:Eu nanowires

Few researchs have been addressed to the photoluminescence and cathodoluminescence of oxide phosphor nanowires. Tin oxide nanowires grown by vapor-liquid-solid process showed the strong UV emission at low temperatures related to the near-band-edge transition.(Chen et al., 2009) Ga_2O_3-SnO_2 nanowires of heterostructure showed a sharp transition region with emission bands from green to red cathodoluminescences.(Maximenko et al., 2009) In Fig. 14A, the photoluminescence (PL) emission spectra of Gd_2O_3:Eu nanowires are compared as a function of heating temperature. As shown in this figure, the emission intensity of Gd_2O_3:Eu nanowires measured at 610 nm is enhanced with increasing the dehydration temperature. When obtained even after dehydration at 800 °C, however, the nanowire phosphor exhibits about 60 % of emission intensity in comparison with that of commercial Y_2O_3:Eu. As pointed out in section 4.1, the high concentration of defects such as stacking faults in the surface of Gd_2O_3:Eu nanowires (Fig. 11c) would act as the nonradiative recombination centers and accordingly be responsible for the low PL emission intensity. The large surface of nanoparticles provides efficient quenching centers for the deexcitation via traps. The density of phonons of the nanoparticles, which is crucial for the resonant energy transfer, is also much lower than that of normal crystal. All of these effects result in a decreased probability of energy transfer among activator ions. As a consequence, higher activator concentrations have been generally observed for the optimized radiative recombination in nanosized particles than in normal materials.(Duan et al., 2000; Zhang et al., 2003) While an increase of the activator concentration improves the probability of the energy transfers to the activator ions and therefore radiative recombination, the probability

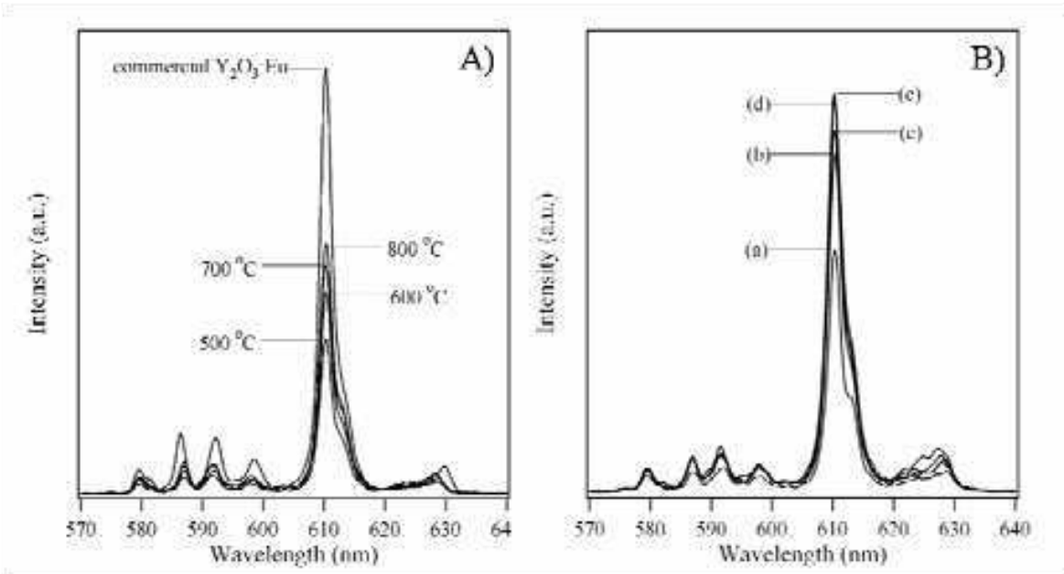

Fig. 14. (A) PL emission spectra (λ_{ex} = 254 nm) of Gd_2O_3:Eu nanowires as a function of heating temperature. All intensities were measured as values relative to that of commercial Y_2O_3:Eu. (B) Comparison of PL emission spectra (λ_{ex} = 254 nm) of $Gd_{2-x}Eu_xO_3$ nanowires as a function of the Eu^{3+} concentration; x = 0.08 (a), 0.12 (b), 0.16 (c), 0.20 (d), and 0.24 (e).

of energy transfer between activator ions also increases to induce a concentration quenching. Because there are no intermediate energy levels between the excited $^5D_0$ state and the ^7F_J states of Eu^{3+} to act as a bridge for cross-relaxation, the concentration quenching effect is essentially ascribed to the possible nonradiative transfer between neighboring Eu^{3+} ions. (Zhang et al., 1998; Dhanaraj et al., 2001) The quenching concentration of Eu^{3+} activators for $Gd_{2-x}Eu_xO_3$ nanowires is determined by measuring the PL intensity in the range of $0.08 \leq x \leq 0.24$. The relationship between photoemission intensity of $^5D_0 - {}^7F_2$ at 610 nm and Eu^{3+} activator concentration (x) for the $Gd_{2-x}Eu_xO_3$ nanowires is shown in Fig. 13B. The quenching concentration for nanowires is in the range $0.16 < x < 0.20$, which is much higher value in comparison with that ($x < 0.08 \sim 0.10$) for the bulk Gd_2O_3:Eu powder. Although the PL intensity of $x = 0.24$ member is comparable to that of $x = 0.20$ member, the nanowire shape is no longer observed and instead the nanospheres or nanorods with low aspect ratios is formed after high temperature annealing (Fig. 12).

5. Conclusion

Gadolinium oxide (Gd_2O_3) with a cubic structure is used as an efficient host matrix for trivalent rare earth ions for the fabrication of nanocrystalline phosphor materials. Because of the high refractive index, the large band gap (5.4 eV), the high resistivity and the high relative permittivity, gadolinium oxide is a promising material for high-*k* gate dielectrics, waveguides, and high resolution X-ray image detectors. Gd^{3+} is also a known contrast agent for magnetic resonance imaging (MRI), and thus the rare-earth doped Gd_2O_3 labels can be used for dual, fluorescence and MR imaging applications. In this chapter, we described that various single crystalline nanostructures (nanorods, nanowires, nanotubes, nanospheres) of red-emitting Gd_2O_3:Eu phosphor can be prepared by selective hydrothermal synthesis of $Gd(OH)_3$:Eu at different pHs and subsequent dehydration at high temperatures. The aspect ratios of phosphor particles are tunable by simply adjusting the pH of the initial solution for hydrothermal synthesis of $Gd(OH)_3$:Eu. In particular, the nanowires of $Gd(OH)_3$:Eu can be selectively prepared at pH ~ 11. Highly uniform nanowires of 20 ~ 30 nm in diameter can grow up to several tens of micrometers in length. The shape of nanowire obtained under hydrothermal pressures are retained after the structural transformation from hexagonal $Gd(OH)_3$:Eu to cubic Gd_2O_3:Eu at high temperatures. Therefore, the selective control of $Gd(OH)_3$:Eu morphology provides a strategy for the selective control of one-dimensional oxide nano-phosphor Gd_2O_3:Eu. This method for the synthesis of Gd_2O_3:Eu nanowires is quite simple and facile. No catalyst is required to serve as the energetically favorable site for the absorption of reactants. No template is added to direct the growth of nanowires. The relative emission intensity of Gd_2O_3:Eu is reduced with increasing the aspect ratio of nanoparticles and the quenching concentration of activators is significantly increased in Gd_2O_3:Eu nanowires ($x = 0.20$) compared with that of the bulk powder ($x = 0.08 \sim 0.10$). Thus, the low luminescence efficiency of Gd_2O_3:Eu nanowires can be highly improved by doping more Eu^{3+} into the host lattice. This compensation of luminescence efficiency would be of great benefit to the practical use of Gd_2O_3:Eu phosphor nanowires.

6. Acknowledgment

The authors acknowledge the grant R01-2008-000-10442-0 from the Korea Science and Engineering Foundation.

7. References

Bae, Y.-J.; Lee, K.-H. & Byeon, S.-H. (2009). Synthesis and Eu^{3+} concentration-dependent photoluminescence of $Gd_{2-x}Eu_xO_3$ nanowires. *J. Lumin.*, 129, 1, (2009) 81-85, ISSN 0022-2313

Beaurepaire, E.; Buissette, V.; Sauviat, M.-P.; Mercuri, A.; Martin, J.-L.; Lahlil, K., Giaume, D.; Huignard, A. Gacoin, T.; Boilot, J.-P. & Alexandrou, A. (2004). Functionalized fluorescent oxide nanoparticles: artificial toxins for sodium channel targeting and imaging at the single-molecule level. *Nano Lett.*, 4, 11, (2004) 2079-2083, ISSN 1530-6984

Birkmire, R.W. & Eser, E. (1997). Polycrystalline thin film solar cells: present status and future potential. *Annu. Rev. Mater. Sci.*, 27, (1997) 625–653, ISSN 0084-6600

Blasse, G. & Grabmaier, B.C. (1994). *Luminescent Materials*, Springer, ISBN 3-540-58019-0, Berlin

Brecher, C.; Samelson, H.; Lempicki, A.; Riley, R. & Peters, T. (1967). Polarized spectra and crystal-field parameters of Eu^{+3} in YVO_4. *Phys. Rev.*, 155, 2, (1967) 178-187, ISSN 0031-899X

Buijs, M.; Meyerink, A. & Blasse, G. (1987). Energy transfer between Eu^{3+} ions in a lattice with two different crystallographic sites: Y_2O_3:Eu^{3+}, Gd_2O_3:Eu^{3+} and Eu_2O_3. *J. Lumin.*, 37,1, (1987) 9-20 , ISSN 0022-2313

Byeon, S.-H.; Ko, M.-G.; Park, J.-C. & Kim, D.-K. (2002). Low-temperature crystallization and highly enhanced photoluminescence of $Gd_{2-x}Y_xO_3$:Eu^{3+} by Li doping. *Chem. Mater.*, 14, 2, (2002) 603-608, ISSN 0897-4756

Chang, C.; Kimura, F.; Kimura, T. & Wada, H. (2005). Preparation and characterization of rod-like Eu:Gd_2O_3 phosphor through a hydrothermal routine. *Mater. Lett.*, 59, 8-9, (2005) 1037-1041, ISSN 0167-577X

Chang, C.; Zhang, Q.; Mao, D. (2006). The hydrothermal preparation, crystal structure and photoluminescent properties of GdOOH nanorods. *Nanotech.*, 17, 8, (2006) 1981-1985 , ISSN 0957-4484

Chen, R.; Xing, G.Z.; Gao, J.; Zhang, Z.; Wu, T. & Sun, H.D. Characteristics of ultraviolet photoluminescence from high quality tin oxide nanowires. *Appl. Phys. Lett.*, 95, (2009) 061908, ISSN 0003-6951

Counio, G.; Gacoin, T. & Boilot, J.-P. (1998). Synthesis and photoluminescence of $Cd_{1-x}Mn_xS$ (x = 5%) nanocrystals. *J. Phys. Chem. B*, 102, 27, (1998) 5257-5260, ISSN 1089-5647

Cuif, J.P.; Rohart, E.; Macaudiere, P.; Bauregard, C.; Suda, E.; Pacaud, B.; Imanaka, N.; Masui, T. & Tamura, S. (2004). *Binary Rare Earth Oxides*, Kluwer Academic Publishers, ISBN 9781402025688, Dordrecht

Dhanaraj, J.; Jagannathan, R.; Kutty, T.R.N. & Lu, C.H. (2001). Photoluminescence characteristics of Y_2O_3:Eu^{3+} nanophosphors pPrepared using sol-gel thermolysis. *J. Phys. Chem. B*, 105, 45, (2001) 11098-11105, ISSN 1089-5647

Du, G. & Van Tendeloo, G. (2005). Preparation and structure analysis of $Gd(OH)_3$ nanorods. *Nanotechnology*, 16, 4, (2005) 595-597, ISSN 0957-4484

Duan, C.K.; Yin, M.; Yan, K. & Reid, M. (2000). Surface and size effects and energy transfer phenomenon on the luminescence of nanocrystalline X_1–Y_2SiO_5:Eu^{3+}. *J. Alloys Compd.*, 303-305, (2000) 371-375, ISSN 0925-8388

Ebbesen, T.W. & Ajayan, P.M. (1992). Large-scale synthesis of carbon nanotubes. *Nature*, 358, 6383, (1992) 220-222, ISSN 0028-0836

El-sayed, M. (2001). Some interesting properties of metals confined in time and nanometer space of different shapes. *Acc. Chem. Res.*, 34, 4, (2001) 257-264, ISSN 0001-4842

Erdei, S.; Roy, R.; Harshe, G.; Juwhari, S.; Agrawal, H. D.; Ainger, F.W. & White, W.B. (1995). The effect of powder preparation processes on the luminescent properties of yttrium oxide based phosphor materials. *Mater. Res. Bull.*, 30, 6, (1995) 745-753, ISSN 0025-5408

Fang, C.; Geng, B.; Liu, J. & Zhan, F. (2009). D-fructose molecule template route to ultra-thin $ZnSnO_3$ nanowire architectures and their application as efficient photocatalyst. *Chem. Commun.*, 2009, 2350–2352, ISSN 1359-7345

Fang, Y.-P.; Xu, A.-W.; Song, R.-Q.; Zhang, H.-X.; You, L.-P.; Yu, J.C. & Liu. H.-Q. (2003). Systematic synthesis and characterization of single-crystal lanthanide orthophosphate nanowires. *J. Am. Chem. Soc.*, 125, (2003) 16025-16034, ISSN 0002-7863

Goldys, E.M.; D.-Tomsia, K.; Jinjun, S.; Dosev, D.; Kennedy, I.M.; Yatsunenko, S. & Godlewski, M. (2006). Optical characterization of Eu-doped and undoped Gd_2O_3 nanoparticles synthesized by the hydrogen flame pyrolysis method. *J. Am. Chem. Soc.*, 128, 45, (2006) 14498-14505, ISSN 0002-7863

Guo, H.; Dong, N.; Yin, M.; Zhang, W.; Lou, L. & Xia, S. (2004). Visible upconversion in rare earth ion-doped Gd_2O_3 nanocrystals. *J. Phys. Chem. B*, 108, 50, (2004) 19205-19209, ISSN 1520-5207

Hirai, T. & Orikoshi, T. (2004). Preparation of Gd_2O_3:Yb,Er and Gd_2O_2S:Yb,Er infrared-to-visible conversion phosphor ultrafine particles using an emulsion liquid membrane system. *J. Colloid Interface Sci.*, 269, 1, (2004) 103-108, ISSN 0021-9797

Hosono, E.; Kudo, T.; Honma, I.; Matsuda, H. & Zhou, H. (2009). Synthesis of single crystalline spinel $LiMn_2O_4$ nanowires for a lithium ion battery with high power density. *Nano Lett.*, 9, 3, (2009) 1045-1051, ISSN 1530-6984

Hu, J.; Odom, T. W. & Lieber, C.M. (1999). Chemistry and physics in one dimension: synthesis and properties of nanowires and nanotubes. *Acc. Chem. Res.*, 32, 5, (1999) 435-445 , ISSN 0001-4842

Iijima, S. (1991). Helical microtubules of graphitic carbon. *Nature*, 354, 6348, (1991) 56-58 , ISSN 0028-0836

Iijima, S. & Ichihashi, T. (1993). Single-shell carbon nanotubes of 1-nm diameter. *Nature*, 363, 6430, (1993) 603-605, ISSN 0028-0836

Jia, C.-J.; Sun, L.-D.; Yan, Z.-G.; You, L.-P.; Luo, F.; Han, X.-D.; Pang, Y.-C.; Zhang, Z. & Yan, C.H. (2005). Single-crystalline iron oxide nanotubes. *Angew. Chem. Int. Ed.*, 44, 28, (2005) 4328-4333, ISSN 0570-0833

Jiang, Y.D.; Wang, Z.L.; Zhang, F.; Paris, H.G. & Summers, C.J. (1998). Synthesis and characterization of Y_2O_3: Eu^{3+} powder phosphor by a hydrolysis technique. *J. Mater. Res.*, 13, 10, (1998) 2950-2955, ISSN 0884-2914

Jing, X.; Ireland, T.; Gibbons, C.; Barber, D.J.; Silver, J.; Vecht, A.; Fern, G.; Trowga, P. & Morton, D.C. (1999). Control of Y_2O_3:Eu spherical particle phosphor size, assembly properties, and performance for FED and HDTV. *J. Electrochem. Soc.*, 146, 12, (1999) 4654-4658, ISSN 0013-4651

Kazes, M.; Lewis, D.Y.; Ebenstein, Y.; Mokari, T. & Banin, U. (2002). Lasing from semiconductor guantum rods in a cylindrical Microcavity. *Adv. Mater.*, 14, 4, (2002) 317-321, ISSN 0935-9648

Khan, M.A.; Jung, H.-T. & Yang, O.-B. (2006). Synthesis and characterization of ultrathin crystalline TiO_2 nanotubes. *J. Phys. Chem. B*, 110, 13, (2006) 6626-6630, ISSN 1520-5207

Law, M.; Greene, L.E.; Johnson, J.C.; Saykally, R. & Yang, P. (2005). Nanowire dye-sensitized solar cells. *Nat. Mater.*, 4, (2005) 455–459, ISSN 1476-1122

Lee, B.-I.; Lee, K.S.; Lee, J.H.; Lee, I.S. & Byeon, S.-H. (2009). Synthesis of colloidal aqueous suspensions of a layered gadolinium hydroxide: a potential MRI contrast agent. *Dalton Trans.*, (2009) 2490-2495, ISSN 1477-9226

Lee, K.-H.; Bae, Y.-J. & Byeon, S.-H. (2009). Nanostructures and photoluminescence properties of Gd_2O_3:Eu red-phosphor prepared via hydrothermal route. *Bull. Kor. Chem. Soc.*, 29, 11, (2008) 2161-2168, ISSN 0253-2964

Lee, K.-H. & Byeon, S.-H. (2009). Extended members of layered rare-earth hydroxide family, $RE_2(OH)_5NO_3 \cdot nH_2O$ (RE = Sm, Eu, and Gd): synthesis and anion-exchange behavior. *Eur. J. Inorg. Chem.*, 2009, 8, (2009) 929-936, ISSN 1434-1948

Leschkies, K.S.; Divakar, R.; Basu, J.; Enache-Pommer, E.; Boercker, J.E.; Carter, C.B.; Kortshagen, U.R.; Norris, D.J. & Aydil, E.S. (2007). Photosensitization of ZnO nanowires with CdSe quantum dots for photovoltaic devices. *Nano Lett.*, 7, (2007) 1793–1798, ISSN 1530-6984

Levy-Clement, C.; Tena-Zaera, R.; Ryan, M.A.; Katty, A. & Hodes, G. (2005). CdSe-sensitized p-CuSCN/nanowire n-ZnO heterojunctions. *Adv. Mater.*, 17, (2005) 1512–1515, ISSN 0935-9648

Liang, J.H. & Li, Y.D. (2003). Synthesis and characterization of $Ni(OH)_2$ single-crystal nanorods. *Chem. Lett.*, 32, 12, (2003) 1126-1127, ISSN 1348-0715

Louis, C.; Bazzi, R.; Flores, M.A.; Zheng, W.; Lebbou, K.; Tillement, O.; Mercier, B.; Dujardin, C. & Perriat, P. (2003). Synthesis and characterization of Gd_2O_3:Eu^{3+} phosphor nanoparticles by a sol-lyophilization technique. *J. Solid State Chem.*, 173, 2, (2003) 335-341, ISSN 0022-4596

Louis, C.; Bazzi, R.; Marquette, C.A.; Bridot, J.L.; Roux, S.; Ledoux, G.; Mercier, B.; Blum, L.; Perriat, P. & Tillement, O. (2005). Nanosized hybrid particles with double luminescence for biological labeling. *Chem. Mater.*, 17, 7, (2005) 1673-1682, ISSN 0897-4756

Magrez, A.; Vasco, E.; Seo, J.W.; Dieker, C.; Setter, N. & Forro, L. (2006). Growth of single-crystalline $KNbO_3$ nanostructures. *J. Phys. Chem. B*, 110, 1, (2006) 58-61, ISSN 1520-5207

Matijevic, E. & Hsu, W.P. (1987). Preparation and properties of monodispersed colloidal particles of lanthanide compounds: I. gadolinium, europium, terbium, samarium, and cerium(III). *J. Colloid Interface Sci.*, 118, 2, (1987) 506-523, ISSN 0021-9797

Maximenko, S. I.; Mazeina, L.; Picard, Y.N.; Freitas, J.A.; Bermudez, Jr., V.M. & Prokes, S. M. Cathodoluminescence studies of the inhomogeneities in Sn-doped Ga_2O_3 nanowires. *Nano Lett.*, 9, 9, (2009) 3245-3251, ISSN 1530-6984

Nichkova, M.; Dosev, D.; Gee, S.J.; Hammock, B.D. & Kennedy, I.M. (2005). Microarray immunoassay for phenoxybenzoic acid using polymer encapsulated Eu:Gd_2O_3 nanoparticles as fluorescent labels. *Anal. Chem.*, 77, 21, (2005) 6864-6873, ISSN 0003-2700

Parilla, P.A.; Dillon, A.C.; Jones, K.M.; Riker, G.; Schulz, D.L.; Ginley, D.S. & Heben, M.J. (1999). The first true inorganic fullerenes? *Nature*, 397, 6715, (1999) 114, ISSN 0028-0836

Rackauskas, S.; Nasibulin, A.G.; Jiang, H.; Tian, Y.; Kleshch, V.I.; Sainio, J.; Obraztsova, E. D.; Bokova, S.N.; Obraztsov, A.N. & Kauppinen, E.I. (2009). A novel method for metal oxide nanowire synthesis. *Nanotech.*, 20, (2009) 165603(8pp), ISSN 0957-4484

Rao, C.N.R. & Nath, M. (2003). Inorganic nanotubes. *J. Chem. Soc., Dalton Trans.*, 1, (2003) 1-24, ISSN 1477-9226

Rao, C.N.R.; Mueller, A. & Cheetham, A.K. (2004). *The Chemistry of Nanomaterials*; Wiley-VCH: Weinheim, ISBN 3527306862, Germany

Ravichandran, D.; Roy, R. & White, W.B. (1997). Synthesis and characterization of sol-gel derived hexa-aluminate phosphors. *J. Mater. Res.*, 12, 3, (1997) 819-824, ISSN 0884-2914

Rossner, W. & Grabmaier, B.C. (1991). Phosphors for X-ray detectors in computed tomography. *J. Lumin.*, 48/49, 1, (1991) 29-36, ISSN 0022-2313

Rossner, W. (1993). The conversion of high energy radiation to visible light by luminescent ceramics. *IEEE Trans. Nucl. Sci.*, 40, 4, (1993) 376-379, ISSN 0018-9499

Sharma, S. & Sunkara, M.K. (2002). Direct synthesis of gallium oxide tubes, nanowires, and nanopaintbrushes. *J. Am. Chem. Soc.*, 124, 41, (2002) 12288-12293, ISSN 0002-7863

Shea, L.E.; McKittrick, J. & Lopez, O.A. (1996). Synthesis of red-emitting, small particle size luminescent oxides using an optimized combustion process. *J. Am. Ceram. Soc.*, 79, 12, (1996) 3257-3265, ISSN 0002-7820

Singh, D.P.; Neti, N. R.; Sinha, A.S.K. & Srivastava, O.N. (2007). Growth of different nanostructures of Cu_2O (nanothreads, nanowires, and nanocubes) by simple electrolysis based oxidation of copper. *J. Phys. Chem. C.*, 111, 4, (2007) 1638-1645, ISSN 1932-7455

Tang, B.; Zhou, L.; Ge, J.; Niu, J. & Shi, Z. (2005). Hydrothermal synthesis of ultralong and single-crystalline $Cd(OH)_2$ nanowires using alkali salts as mineralizers. *Inorg. Chem.*, 44, 8, (2005) 2568-2569, ISSN 0020-1669

Tang, C.; Bando, Y.; Liu, B. & Goldberg, D. (2005). Cerium oxide nanotubes prepared from cerium hydroxide nanotubes. *Adv. Mater.*, 17, 24, (2005) 3005-3009, ISSN 0935-9648

Tenne, R. (1995). Doped and heteroatom-containing fullerene-like structures and nanotubes. *Adv. Mater.*, 7, 12, (1995) 965-995, ISSN 0935-9648

Velazquez, J.M. & Banerjee, S. (2009). Catalytic growth of single-crystalline V_2O_5 nanowire arrays. *Small*, 5, 9, (2009) 1025–1029, ISSN 1613-6810

Wang, X. & Li, Y. (2002). Synthesis and characterization of lanthanide hydroxide single-crystal nanowires. *Angew. Chem. Int. Ed.*, 41, 24, (2002) 4790-4793, ISSN 0570-0833

Wang, X.; Sun, X; Yu, D.; Zou, B & Li, Y. (2003). Rare earth compound nanotubes. *Adv. Mater.*, 15, 17, (2003) 1442-1445, ISSN 0935-9648

Wang, X. & Li, Y. (2003). Rare-earth-compound nanowires, nanotubes, and fullerene-like nanoparticles: synthesis, characterization, and properties. *Chem. Eur. J.*, 9, (2003) 5627-5635, ISSN 0947-6539

Xia, Y.N.; Yang, P.D.; Sun, Y.G.; Wu, Y.Y.; Mayers, B.; Gates, B.; Yin, Y.D.; Kim, F. & Yan, Y.Q. (2003). One-dimensional nanostructures: synthesis, characterization, and applications. *Adv. Mater.*, 15, 5, (2003) 353-389, ISSN 0935-9648

Xu, G.; Ren, Z.; Du, P.; Weng, W.; Shen, G. & Han, G. (2005). Polymer-assisted hydrothermal synthesis of single-crystalline tetragonal perovskite $PbZr_{0.52}Ti_{0.48}O_3$ nanowires. *Adv. Mater.*, 17, 7, (2005) 907-910, ISSN 0935-9648

Yan, M.F.; Huo, T.C. D. & Ling, H.C. (1987). Preparation of $Y_3Al_5O_{12}$-based phosphor powders. *J. Electrochem. Soc.*, 134, 2, (1987) 493-498, ISSN 0013-4651

Yan, R.; Sun, X.; Wang, X., Peng, Q. & Li, Y. (2005). Crystal structures, anisotropic growth, and optical properties: Controlled synthesis of lanthanide orthophosphate one-dimensional nanomaterials. *Chem. Eur. J.*, 11, (2005) 2183-2195, ISSN 0947-6539

Yen, W.M.; Shionoya, S. & Yamamoto, H. (2007). *Phosphor Handbook*, CRC Press, ISBN 0-8493-3564-8, New York

Zhang, W.P.; Xie, P.B.; Duan, C.K.; Yan, K.; Yin, M.; Lou, L.R.; Xia, S.D. & Krupa, J.C. (1998). Preparation and size effect on concentration quenching of nanocrystalline Y_2SiO_5:Eu. *Chem. Phys. Lett.*, 292, 1-2, (1998) 133-136, ISSN 0009-2614

Zhang, W.W.; Zhang, W.P.; Xie, P.B.; Yin, M.; Chen, H.T.; Jing, L.; Zhang, Y.S.; Lou, L.R. & Xia, S.D. (2003). Optical properties of nanocrystalline Y_2O_3:Eu depending on its odd structure. *J. Colloid Interface Sci.*, 262, 2, (2003) 588-593, ISSN 0021-9797

Zhou, Y.; Lin, J. & Wang, S. (2003). Energy transfer and upconversion luminescence properties of Y_2O_3:Sm and Gd_2O_3:Sm phosphors. *J. Solid State Chem.*, 171, 1-2, (2003) 391-395, ISSN 0022-4596

Nanowires Science and Technology

Edited by Nicoleta Lupu

ISBN 978-953-7619-89-3
Hard cover, 402 pages
Publisher InTech
Published online 01, February, 2010
Published in print edition February, 2010

This book describes nanowires fabrication and their potential applications, both as standing alone or complementing carbon nanotubes and polymers. Understanding the design and working principles of nanowires described here, requires a multidisciplinary background of physics, chemistry, materials science, electrical and optoelectronics engineering, bioengineering, etc. This book is organized in eighteen chapters. In the first chapters, some considerations concerning the preparation of metallic and semiconductor nanowires are presented. Then, combinations of nanowires and carbon nanotubes are described and their properties connected with possible applications. After that, some polymer nanowires single or complementing metallic nanowires are reported. A new family of nanowires, the photoferroelectric ones, is presented in connection with their possible applications in non-volatile memory devices. Finally, some applications of nanowires in Magnetic Resonance Imaging, photoluminescence, light sensing and field-effect transistors are described. The book offers new insights, solutions and ideas for the design of efficient nanowires and applications. While not pretending to be comprehensive, its wide coverage might be appropriate not only for researchers but also for experienced technical professionals.

InTech Europe
University Campus STeP Ri
Slavka Krautzeka 83/A
51000 Rijeka, Croatia
Phone: +385 (51) 770 447
Fax: +385 (51) 686 166
www.intechopen.com

InTech China
Unit 405, Office Block, Hotel Equatorial Shanghai
No.65, Yan An Road (West), Shanghai, 200040, China
中国上海市延安西路65号上海国际贵都大饭店办公楼405单元
Phone: +86-21-62489820
Fax: +86-21-62489821

IntechOpen